Detection of Neutron Irradiation-Induced Crystal Defects in Silicon with Photoluminescence, Deep Level Transient Spectroscopy and Dark Current Measurements on CMOS Image Sensors

Juan Esteban Montoya Cardona, Sylvain Joblot, Richard Monflier, Éric Imbernon, Aubin Antonsanti, Alexandre Le Roch, Olivier Marcelot, Vincent Goiffon

Detection of Neutron Irradiation-Induced Crystal Defects in Silicon with Photoluminescence, Deep Level Transient Spectroscopy and Dark Current Measurements on CMOS Image Sensors

Juan Esteban Montoya Cardona, Sylvain Joblot, Richard Monflier, Eric Imbernon, Aubin Antonsanti, Alexandre Le Roch, Olivier Marcelot and Vincent Goiffon

***Abstract*—Defects generated in the bulk silicon following displacement damage induced by fast neutrons irradiation are characterized using the dark current spectroscopy (DCS), deep level transient spectroscopy (DLTS) and photoluminescence (PL) techniques, the latter of which has been scarcely used in this context. Irradiations with fluences of at least 1×10^{10} cm^{-2} were sufficient to generate an exponential tail of white pixels in the DCS distributions of CMOS image sensors (CIS), with the DCS-extracted activation energy being close to midgap for high dark current values, suggesting the presence of complex defect clusters. PL and DLTS measurement required respectively fluences 10 and 5 times higher to obtain spectral signatures of point defects such as C_iO_i, C_iC_s and the di-vacancy. Simulations based on a simplified model suggest that the exponential tail observed in DCS for clusters can be explained by an exponential distribution both of cluster sizes and capture cross section values, as long as the cluster introduces at least an energy level close to midgap. The three techniques provide useful and complementary information for the characterization of irradiation-induced defects.**

***Keywords*—Dark Current, Deep Level Transient Spectroscopy, Neutron Irradiation, Photoluminescence, Silicon.**

Manuscript submitted 13 September 2024.

Juan Esteban Montoya Cardona is with ISAE-SUPAERO, 31400 Toulouse, France, also with LAAS-CNRS, 31400 Toulouse, France, and also with STMicroelectronics, 38920 Crolles, France (e-mail: Juan.MONTOYA-CARDONA@isae-supaero.fr).

Sylvain Joblot is with STMicroelectronics, 38920 Crolles, France (e-mail: sylvain.joblot@st.com).

Richard Monflier and Eric Imbernon are with LAAS-CNRS, 31400 Toulouse, France (e-mail: richard.monflier@laas.fr).

Aubin Antonsanti, Alexandre Le Roch, Olivier Marcelot and Vincent Goiffon are with ISAE-SUPAERO, 31400 Toulouse, France (e-mail: vincent.goiffon@isae-supaero.fr).

I. Introduction

THE use of CMOS image sensors (CIS) has become widespread for various applications, ranging from consumer products to specialized scientific and industrial applications. In the case of CIS developed for applications in the space and nuclear sectors, these devices must be designed and manufactured so as to maintain their electro-optical performance (in particular their dark current levels) even under radiation by highly energetic particles such as neutrons. Irradiation with neutrons has the particularity of generating predominantly displacement damage in the bulk silicon, with the total ionizing dose being relatively negligible in comparison [1]. The dark current increase is therefore induced by the presence of point or extended defects in the volume. In order to improve the understanding and prediction of this dark current increase, it appears necessary to identify these bulk defects and their densities. The dark current spectroscopy (DCS) and deep level transient spectroscopy (DLTS) techniques have already been extensively used in the literature with this goal [2-6]. This study aims to compare the DLTS and dark current signatures of electrically active irradiation-induced defects with the signatures of optically active defects induced in the material under the same conditions using the photoluminescence (PL) spectroscopy technique, for which the references in the literature are scarcer.

II. Experimental Details

A. Description of devices and samples

The dark current was characterized using CIS test chips consisting of matrices of pixels, previously fabricated on the same silicon wafer.

Samples for PL measurements were extracted from two Si P-type wafers. Both wafers had the same Cz P-type substrate, doped with boron ($\sim 5.8 \times 10^{14}$ cm^{-3}) and with non-negligible concentrations of oxygen ($\sim 6.5 \times 10^{17}$ cm^{-3}) and carbon ($< 2.5 \times 10^{16}$ cm^{-3}). One of these wafers (substrate A, samples P01-P06) had an oxide layer of ~2.4 nm and was processed with the same N-type and P-type ion implantations forming the photodiode junction of the test chips, as well as a representative Spike annealing. The second wafer (substrate B, samples P07-P12) only had a native oxide layer, and no implantation nor annealing steps.

Samples for DLTS measurements are commercial silicon PIN photodiodes (intrinsic region sandwiched between P-type and N-type regions), with nominal dark current of 0.1 nA at a reverse voltage of V_R = 20 V. Although these photodiodes are not processed with the same process flow as the test chips, they are expected to be representative of a similar advanced imaging process.

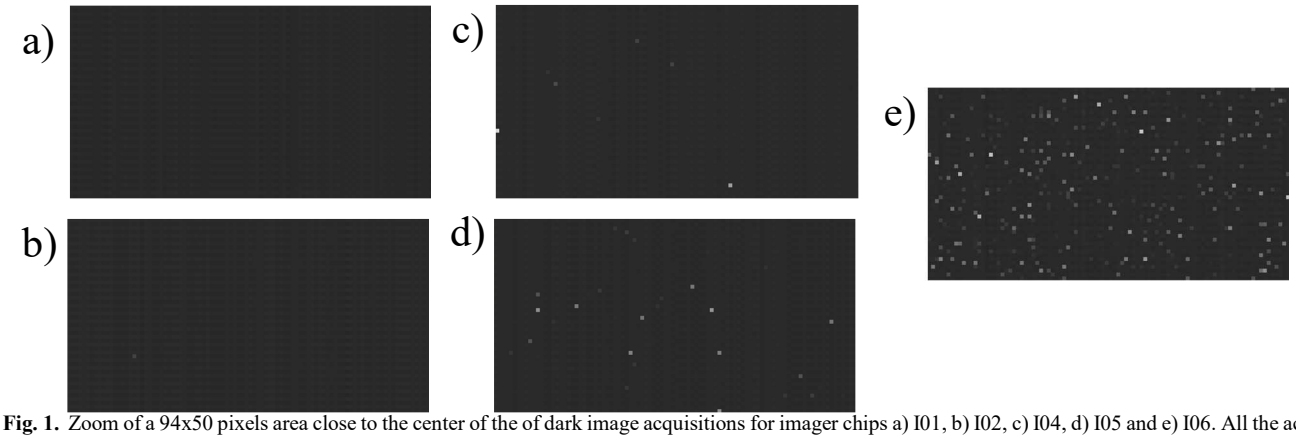

Fig. 1. Zoom of a 94x50 pixels area close to the center of the of dark image acquisitions for imager chips a) I01, b) I02, c) I04, d) I05 and e) I06. All the acquisitions were done at a temperature of 67 °C and with an integration time of 15 ms.

B. Neutron irradiation conditions

The image sensor chips, PL samples and PIN photodiodes were irradiated with neutrons at the Cyclotron Resources Centre at UCL (Université Catholique de Louvain). The CIS and the PIN photodiodes were unbiased during the irradiation. The neutron beam had a conical shape and consisted of a continuous neutron energy spectrum centered on 23 MeV. Table I summarizes the irradiation conditions for the samples and the devices.

Table I
Neutron irradiation conditions

CIS test chip	PL sample	PIN photodiode	Neutron fluence [cm^{-2}]	Neutron flux [$cm^{-2}s^{-1}$]
I01	P05, P11, P06, P12	D01	0	0
I02, I03	P01, P07		1×10^{9}	5×10^{6}
I04	P02, P08		1×10^{10}	2×10^{7}
		D02	1×10^{10}	1×10^{7}
		D03	5×10^{10}	1×10^{7}
I05	P03, P09		1×10^{11}	2×10^{8}
		D04	1×10^{11}	1×10^{7}
I06, I07	P04, P10		1×10^{12}	2×10^{8}

Following the irradiation, samples were stored under controlled room temperature in dry air before any measurement.

C. Characterization

The electro-optical characterization of the CIS was conducted using a bench with an LED light source. The temperature at the silicon bulk was estimated by an average of four temperature sensors integrated into the test chips, with a calibration offset. Before irradiation, all of the test chips were characterized at a single temperature (67 °C). 6 weeks after the irradiation, the test chips were characterized at different temperatures ranging from 23 °C to 67 °C, as well as an additional 83 °C measurement for I06, with different integration times for the dark current extraction. Each dark image consists of an average of 100 consecutive acquisitions.

PL measurements were performed 17 weeks after the irradiation at 9 K with an ARS Helium cryostat. An excitation laser of 488 nm wavelength was used. The luminescence was collected by a 10X 0.26 NA objective and analyzed with an S&I MonoVista spectrometer integrating an Andor InGaAs detector. The raw spectra were corrected in intensity using as a reference the spectrum emitted by a halogen lamp.

DLTS measurements were conducted 21 weeks after irradiation. The I-V behavior at room temperature of the PIN photodiodes was first measured without illumination. Afterwards, the photodiodes were inserted in a liquid nitrogen cryostat able to cool down the samples to about 85 K. DLTS spectra were obtained in standard capacitance (C-DLTS) mode, the temperature varying from 85 K to 300 K. The diodes were initially biased at a voltage of -25 V (under maximum reverse voltage), followed by a pulse voltage of -0.01 V. with varying pulse widths and time windows.

III. Results

A. Dark current results

Fig. 1 shows a zoomed area of dark image acquisitions at 67 °C and 15 ms integration time for test chips irradiated at different fluences, showing an absence of white pixels for the non-irradiated and lowest-dose irradiated chips (I01 and I02), and a progressive increase in the number of white pixels for the test chips irradiated with fluences between 1×10^{10} cm^{-2} and 1×10^{12} cm^{-2}, suggesting that doses up to 1×10^{9} cm^{-2} do not have an appreciable impact on the number of hot pixels in the device.

For the estimation of the dark current distributions, two different integration times were used for each chip and at each temperature: a constant t_{short} = 400 µs and a variable t_{long} varying from 15 ms to 1000 ms, corresponding to the maximum integration that avoids a saturation of the distribution.

Fig. 2 illustrates a comparison of the dark current distributions for test chips I01-I07 at 67 °C. The histograms of chips I06 and I07 are practically superimposed, confirming that the differences in the dark current levels are caused by the neutron irradiations themselves, and not by potential manufacturing process variability. The distributions of CIS irradiated with at least 1×10^{10} cm^{-2} clearly show the presence of an exponential tail of hot pixels, confirming the increased amounts of white pixels observed in Fig. 1.

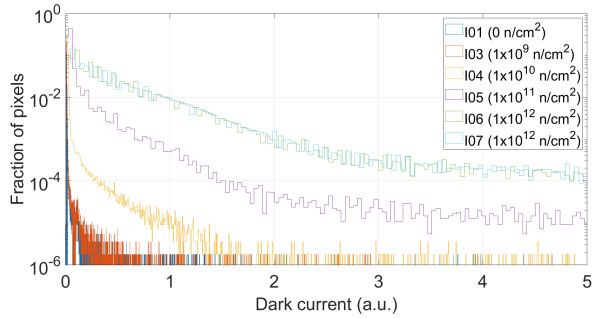

Fig. 2. Dark current distributions of CIS I01-I07 (I02 omitted) at 67 °C, with a dark current cutoff value of 5 a.u.

A comparison of the dark current distributions obtained at different temperatures for CIS I06 is shown in Fig. 3. The exponential tail is present even at the lowest temperature (23 °C), and at the highest temperature (83 °C) two tails with different slopes are visible, with the first slope likely corresponding to diffusion current [2,7]. Fig. 4 shows an activation energy scatter plot for this same chip. The figure shows the presence of two peaks at around 1.15 eV and 0.75 eV, with the former corresponding to pixels in the diffusion regime, with activation energy close to the bandgap energy. Most of the hot pixels in the exponential tail seem to tend towards 0.75 eV, relatively close to the middle of the Si bandgap, suggesting the presence of complex defect clusters with a continuum of different generation rates [8].

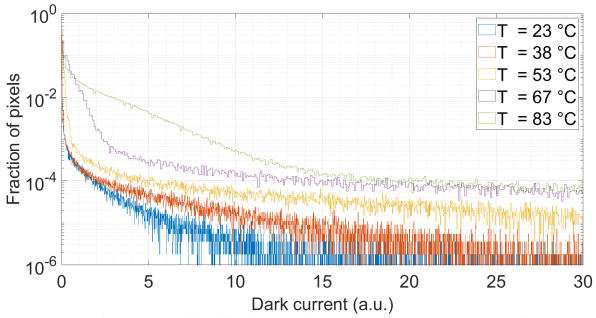

Fig. 3. Dark current distributions of CIS I06 at temperatures between 23 °C and 83 °C, with a dark current cutoff value of 30 a.u.

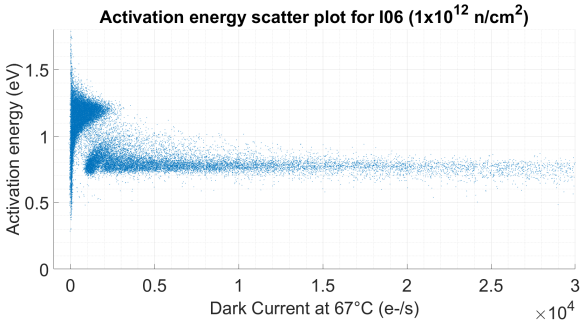

Fig. 4. Activation energy scatter plot for I06 as a function of dark current level at 67 °C (cutoff at 30 a.u.). Only points with $R^2 > 0.999$ are shown.

B. Deep Level Transient Spectroscopy results

DLTS spectra obtained using a filling time of 10 ms and a time window of 100 ms for diodes D01-D04 are displayed in Fig. 5. Despite the relatively low signal-to-noise ratio in the points at higher temperatures, the spectra show the clear presence of two peaks at ~100 K and ~200 K which increase in intensity with irradiation fluence, suggesting the signature of irradiation-induced defects.

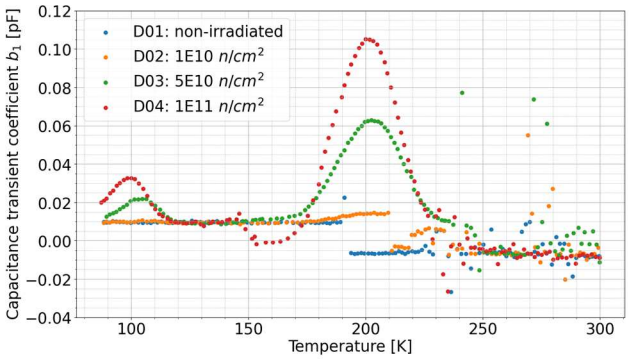

Fig. 5. DLTS spectra for photodiodes D01-D04 (U_R=-25 V, U_P=-0.01 V, t_P=10 ms, t_W=100 ms) between 85 K and 300 K, with b_1 corresponding to one of the Fourier coefficients of the capacitance transient *[9]*.

The spectrum for D04 having the highest peak intensities is used to extract trap defect parameters such as the activation energy, useful for their identification. As indicated in [9], the DLTFS (Deep Level Transient Fourier Spectroscopy) method can be used to deduce the emissivity (e_n) associated with each transient, and to trace an Arrhenius plot allowing the estimation of the activation energy of the traps. Spectra obtained with different filling times (t_P) and time windows (t_W) provide different peaks, as summarized in Table II. In the case of the 200 K peak, the hypothesis of two different slopes can be considered, insinuating the possible presence of 2 peaks very close to each other.

Table II
Activation energies calculated from DLTS spectra.

Conditions	Peak position	Activation energy	Comment
t_W = 100 ms, t_P = 10 ms	~200 K	0.116 eV / 0.231 eV	2 slopes hypothesis
t_W = 100 ms, t_P = 1 ms	~200 K	0.264 eV	1 slope hypothesis
t_W = 100 ms, t_P = 10 ms	~100 K	0.060 eV ± 0.016 eV	1 slope hypothesis
t_W = 1000 ms, t_P = 1 ms	~188 K	0.247 ± 0.042 eV	1 slope hypothesis

The peak observed at ~200 K with t_W = 100 ms and the peak observed at ~188 K with t_W = 1000 ms have similar activation energies, which decrease with larger t_P (0.247 – 0.264 eV / 0.231 eV), possibly related to the saturation of the DLTS signal at a certain t_P value [10,11]. Values reported in the literature [4,5,11] suggest that the defect responsible for this peak might be the di-vacancy in its double-charged state. For t_W = 100 ms, increasing the filling time from 1 ms to 10 ms makes a second slope appear with activation energy of around 0.116 eV, suggesting that there is enough time to fill not only this divacancy, but also an additional defect , which might be a C_i defect acting as an electron trap [4]. On the other hand, the peak observed at ~100 K only for t_W = 100 ms leading to an activation around 0.060 eV might be associated with a C_iC_s defect acting as a hole trap [4].

C. Photoluminescence results

No remarkable differences were observed in the band-to-band (B2B) spectral region besides a decrease in the intensity of the main peak at ~1148 nm with increasing neutron fluence, indicating a degradation of the crystal quality (not shown). A bandpass filter was thus used to reduce the signal under 1200 nm induced by this B2B contribution. Fig. 6 shows PL spectra for samples P01-P06, with the clear presence of two peaks appearing only in the samples irradiated at the highest fluences (P02–P04): a higher intensity peak at ~1570 nm (790 meV), and a lower intensity peak at ~1560 nm (795 meV). It is suspected that the peaks' intensity is linked to the irradiation fluence. Fig. 7 shows how the relative intensity of these two peaks evolves as a function of measurement temperature. In both cases, the intensity increases up until a certain temperature (30 K for the 1570 nm peak, 35 K for the 1560 nm peak), after which the peaks rapidly decrease in intensity until being annihilated around 80 K.

The peak observed at ~1570 nm in the PL spectra of neutron-irradiated samples P02-P04 (Fig. 6) has already been reported in the literature [12-15] as the so-called C-line, which is confidently associated to a C_iO_i defect (a complex of a carbon and an oxygen atom, both situated at interstitial sites), with its intensity increasing with particle irradiation fluence. This identification is supported by the fact that this peak was observed in samples of both substrates A and B, suggesting that it does not strongly depend on the presence of dopant impurities.

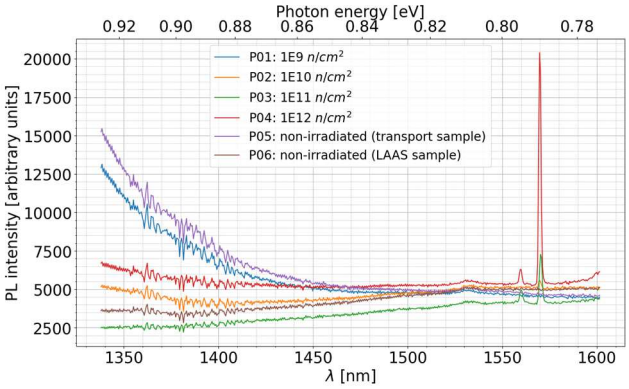

Fig. 6. PL spectra of samples P01-P06 at 9 K in the 1338-1602 nm region, using a laser with a wavelength of 488 nm at 200 mW. The increase in intensity below 1450 nm is caused by the influence of the B2B region.

The identification of the defect responsible for the peak at ~1560 nm is more delicate, although the similarities in the behaviors of both peaks seem to suggest a common origin. [13] reports indeed the presence of a line at 795 meV (corresponding to 1560 nm), which the authors associate with excited electrons in the 1s orbital of the same C_iO_i defect structure. The fact that this peak annihilated at the same temperature as the 1570 nm peak (Fig. 7) supports this hypothesis.

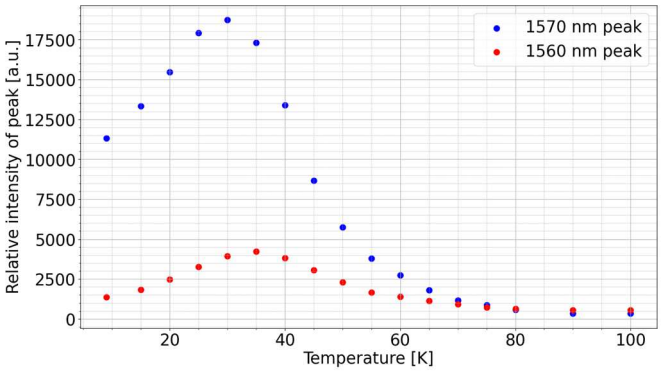

Fig. 7. Intensity of 1570 nm and 1560 nm peaks in the P04 spectrum as a function of temperature. The relative intensity is estimated as the difference between the absolute intensities and a baseline intensity at around 1580 nm.

IV. Discussion

The aforementioned results show that irradiations with fast neutrons can generate sufficient displacement damage in the silicon lattice to favor the formation of a high enough concentration of point defects that can be detected owing to their spectroscopic signatures via the PL and DLTS techniques. With the conditions used experimentally, the observation of defect signatures required neutron fluences of at least 1×10^{11} cm^{-2} to obtain clear defect peaks in the PL spectra, and of at least 5×10^{10} cm^{-2} to obtain clear peaks in the case of DLTS spectra. This contrasts with the degradation observed in the CIS themselves, for which the presence of an exponential tail of white pixels was already evident with neutron fluences as low as 1×10^{10} cm^{-2}. The DCS technique seems therefore to be more sensitive to the presence of crystal defects in the active volume of the material, owing in part to the high number of pixels in the CIS matrix. Nonetheless, the identification of these defects using CIS alone can be quite challenging as was the case in this study, since no discrete peaks in the hot tail section of the dark current distributions were observed, with most of these hot pixels having a relatively constant activation energy close to the middle of the silicon bandgap.

The defects detected with our PL and DLTS data are relatively shallow [4], with energy levels close to the valence or conduction bands, and thus more than likely not responsible for the long exponential tails observed in the dark current distributions of irradiated CIS, which are suspected to be primarily caused by complex clusters of interstitials or vacancies, as expected for samples that have not been annealed at high temperatures post-irradiation [1,3]. To better understand what kinds of defects can potentially be detected via the three spectroscopy techniques, a modeling of the spectra using certain approximations can be useful.

A. Modeling of dark current spectra

An initial estimation of the dark current spectrum generated by a given matrix of active pixels can be obtained by taking into account certain suppositions:

1. For a given defect, the capture cross sections of electrons

and holes are approximately the same.
2. Electric field amplification phenomena such as the Poole-Frenkel and phonon-assisted tunneling effects are neglected.
3. The energy of the bottom of the conduction band is considered to be 0 eV by default, with the energy of a trap given as a negative value with respect to it.

Given this, according to the Shockley-Read-Hall (SRH) theory, the dark current generated by a single defect with energy level E_T and capture cross section σ_n is calculated as [16]:

$$I_{Dark,1} = \frac{q \cdot \sigma_n \cdot v_n \cdot n_i}{2\cosh\left(\frac{|E_T - E_i|}{kT}\right)} \quad (1)$$

$$n_i = \sqrt{N_c N_v} \cdot exp\left(-E_g/2kT\right) \quad (2)$$

with q the electron charge, v_n the thermal velocity of electrons, n_i the intrinsic carrier concentration, E_i the intrinsic Fermi level, k the Boltzmann constant, T the absolute temperature, E_g the bandgap energy and $N_c N_v$ the product of the effective densities of states in the conduction and valence bands, respectively. It is important to remember that some of these quantities depend on the temperature themselves: $v_n \propto T^{1/2}$ and $N_c, N_v \propto T^{3/2}$, as specified in [16].

Starting with the case of point defects, previous studies have shown that the number of individual defects in a given pixel can be described using a Poisson distribution [17]:

$$P_\lambda(N = k) = \frac{\lambda^k}{k!} \cdot e^{-\lambda} \quad (3)$$

where λ corresponds to the mean number of defects per pixel.

Therefore, pixels with $N = 1, 2, 3, \ldots$ defects of the same type will generate a dark current value of:

$$I_{Dark,N} = I_{Dark,0} + N \cdot I_{Dark,1} \quad (4)$$

where $I_{Dark,0}$ is the intrinsic dark current value and $I_{Dark,1}$ is given by (1).

As proposed in [18], to better represent experimental DCS spectra in which the peaks widen for increasing N, the dark current generated by a given pixel can be simulated as a value in a gaussian distribution with mean $I_{Dark,N}$ and variance σ_N^2 given by:

$$\sigma_N^2 = \sigma_0^2 + N \cdot \sigma_T^2 \quad (5)$$

with σ_0^2 the variance of the intrinsic peak, and σ_T^2 the contribution of the traps.

Under these circumstances, a dark current histogram can be simulated for a given population of point defects of interest. Fig. 8 shows the dark current spectra simulated at 67°C for a 1-megapixel matrix containing only two point defects: di-vacancies (V_2) or C_iO_i defects. For this example, the respective mean numbers (λ) of V_2 and C_iO_i defects per pixel are arbitrarily chosen as 5 and 2, respectively. V_2 is considered in a (--/-) charge state, whereas C_iO_i is considered in a (0/+) charge state, with E_T and σ_n values taken from [4]. In these states, the $I_{Dark,1}$ value contributed by each defect is considerably higher for the C_iO_i defect, and thus only the discretization of its peaks is visible at the scale of the figure. The total histogram, assuming pixels simultaneously and uniquely populated by these same two defect populations, retains the same C_iO_i defect peaks, although slightly shifted to the right due to the V_2 contribution. In practical terms, this quantization can only be observed when the average number of traps per pixel is sufficiently low [18].

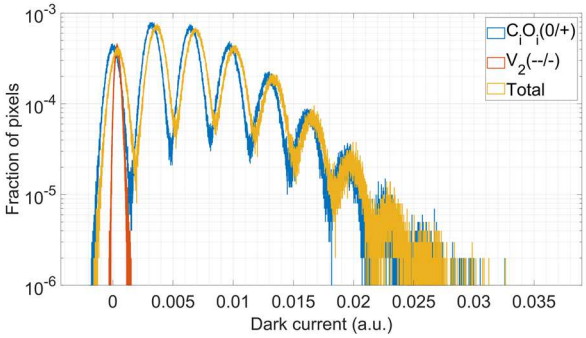

Fig. 8. Simulated dark current distributions at 67 °C for a 1-megapixel image sensor containing V_2 (--/-) and C_iO_i (0/+) defects, with λ of 5 and 2, respectively. Trap parameters are taken from [4]: (E_T, σ_n) = (-0.23 eV, 4.0x10^{-15} cm^2) and (-0.36 eV, 1.9x10^{-15} cm^2), respectively.

Likewise, a similar development can be proposed for the case of defect clusters present inside the active volume of each pixel, under certain assumptions. Supposing a particle irradiation of high enough fluence, it can be reasonably assumed that each pixel can contain at least one defect cluster. For our purposes, we consider as a *cluster* any set of N individual point defects with $N \geq 1$; therefore, this definition includes, among others, self-interstitials, monovacancies and monoatomic impurities for $N = 1$, as well as Frenkel pairs and divacancies for $N = 2$. As a simplification, let us assume that each pixel contains only one cluster, for which N is described by an exponential distribution with mean λ, rounded to the nearest integer value:

$$P_\lambda(N = round(k)) = \frac{1}{\lambda} \cdot e^{-\frac{k}{\lambda}} \quad (6)$$

For a given cluster, let us assume that each of the point defects within can have randomly assigned values of E_T and σ_n, where E_T follows a continuous uniform distribution between $E_v = -1.12$ eV and $E_c = 0$ eV, and σ_n follows as well an exponential distribution with mean μ:

$$P_\mu(\sigma_n = k) = \frac{1}{\mu} \cdot e^{-k/\mu} \quad (7)$$

In this first approximation, it is assumed that each of the point defects inside a cluster is independent from each other, and that it generates a dark current value $I_{Dark,i}$ calculated from its randomly assigned $E_{T,i}$ and $\sigma_{n,i}$ values, using (1). The largest value is considered to be the dark current of the entire cluster:

$$I_{Dark,Cluster} = \max(I_{Dark,i}) \quad (8)$$

Fig. 9 shows above an example of dark current distributions predicted by this model, using three different values of $N_{mean} = \lambda$, as well as a single σ_{mean} value of 1×10^{-15} cm^2, with an order of magnitude representative of values found in the literature [4]. The choice of the three N_{mean} shown in Fig. 9 is justified from the expected sizes of clusters several weeks after irradiation. Indeed, it is possible to calculate the displacement damage dose (DDD) for a given neutron fluence, when considering the energy of the incoming neutrons. Despite the fact that the energy beam was not monoenergetic in our case, the nonionizing energy loss (NIEL) is almost constant in the

energy range centered at 23 MeV; using thus a NIEL value of 4 keV.cm^2/g for 23 MeV neutrons, a DDD value of 4000 TeV/g is obtained for a neutron fluence of 1×10^{11} cm^{-2} [19,20], the highest fluence used in our study. From this DDD, we can obtain the total energy deposited after neutron irradiation in the bulk silicon, using the silicon density and the depletion volume. Dividing this total energy by the threshold displacement energy necessary to eject silicon atoms from their crystalline sites (20 eV [21]), we can get an estimation of the total number of interstitials present in the volume right after irradiation. Assuming a depletion volume in the order of 1 µm^3, this results in about 466 interstitials for a DDD of 4000 TeV/g. This is in good agreement with theoretical estimations representative of the damage state in silicon, several milliseconds after irradiation, using molecular dynamics and the kinetic activation relaxation technique, as reported in [22]. When taking into account the evolution after one minute, this number is generally expected to be divided approximately by a factor of 10 [22], resulting in values similar to the N_{mean} shown in Fig. 9. This is considered to be a good enough approximation in our case, due to the logarithmic-like evolution of the dark current annealing factor in time [23].

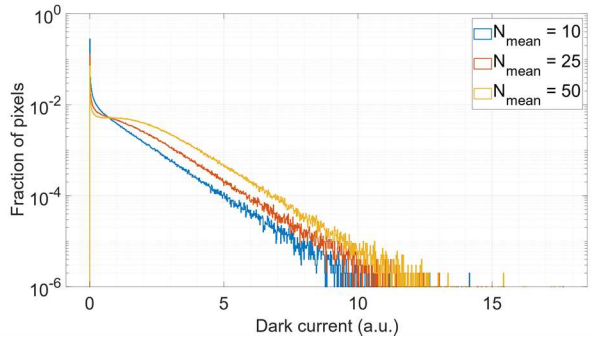

Fig. 9. Simulated dark current distributions at 67 °C for a 1-megapixel image sensor containing 1 cluster per pixel, with 3 different average numbers of defects per cluster. Each defect in a cluster has randomly assigned values of E_T (uniform distribution between $= -1.12$ eV and 0 eV) and σ_n (exponential distribution with a mean value of 1×10^{-15} cm^2).

It can be observed that, under the aforementioned assumptions, the exponential distributions of both N and σ_n result in the presence of an exponential tail of hot pixels. As an illustration, the effects of varying the σ_{mean} values and the E_T ranges are shown in Fig. 10 and Fig. 11, respectively, with the blue curves in Figs. 9, 10 and 11 being analogous. The slope seems to depend strongly on the selected value of σ_{mean}. Comparatively, increasing the N_{mean} or constraining the E_T to only energies close to midgap seem to have a similar albeit weak effect on this slope, with the maximum dark current value being only slightly increased. N only needs to be large enough to have a significant probability of randomly drawing an E_T value close to midgap, whose generation dark current will dominate. If the midgap is artificially excluded from the E_T range, then the distribution collapses to much lower values of dark current, potentially facilitating the observation of discretized point defect peaks such as those in Fig. 8, if these defects are sufficiently separated from the clusters, and in low enough concentrations. This is however very unlikely, as clusters are expected to include energy levels close to midgap, as shown in Fig. 4.

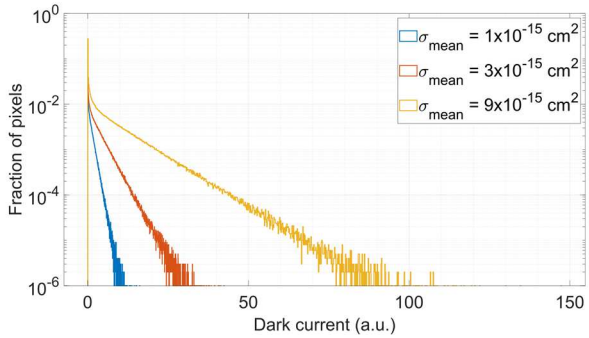

Fig. 10. Simulated dark current distributions at 67 °C under the same conditions as in Fig. 9, but with constant $N_{mean} = 10$, and three different possible values of σ_{mean}, as indicated.

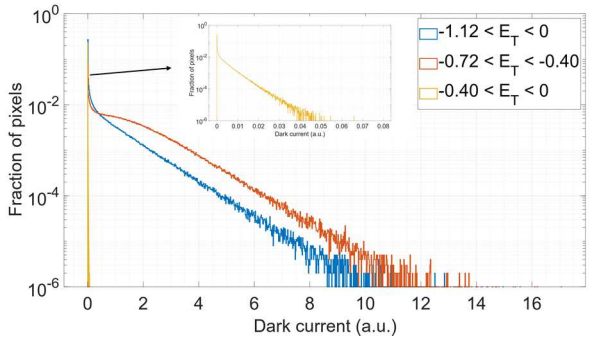

Fig. 11. Simulated dark current distributions at 67 °C under the same conditions as in Fig. 9, but with constant $N_{mean} = 10$, and three different possible ranges for E_T, as indicated in eV. Inset shows zoom at the beginning of the distribution for -0.40 eV $< E_T <$ 0 eV (close to conduction band minimum and excluding midgap).

Fig. 12 includes a comparison between the dark current distributions that can be obtained with this model and those obtained experimentally, in particular at the highest considered neutron fluence (CIS I06 and I07). The figure also includes the implementation of a model for displacement damage-induced dark current, as has already been presented in [24,25]. This latter model, labelled in Fig. 12 as "DDD Model", has been shown to accurately predict the slope of the exponential tail of hot pixels [3]. The free parameter in our model that has the largest influence in this slope is σ_{mean}, as evident when contrasting the above and below sections of Fig. 12. For σ_{mean} of 1×10^{-15} cm^2, only the leftmost part of the distribution is somewhat accurately represented, although this region under about 3 a.u. is attributed to the diffusion regime. To better represent the slope in the SRH generation regime for much larger dark current values, an increase of around a factor of 100 is needed for σ_{mean}. This is somewhat coherent with previous theoretical studies based on ab initio calculations which predict an electronic cross section for clusters several orders of magnitude higher than that of individual point defects [26]. Using this larger σ_{mean} value, however, results in our model significantly overestimating the number of white pixels. Despite this, we can consider that the blue curve in Figs. 9, 10 and 11 constitutes a qualitatively suitable representation for the

dark current histogram related to irradiation-induced clusters.

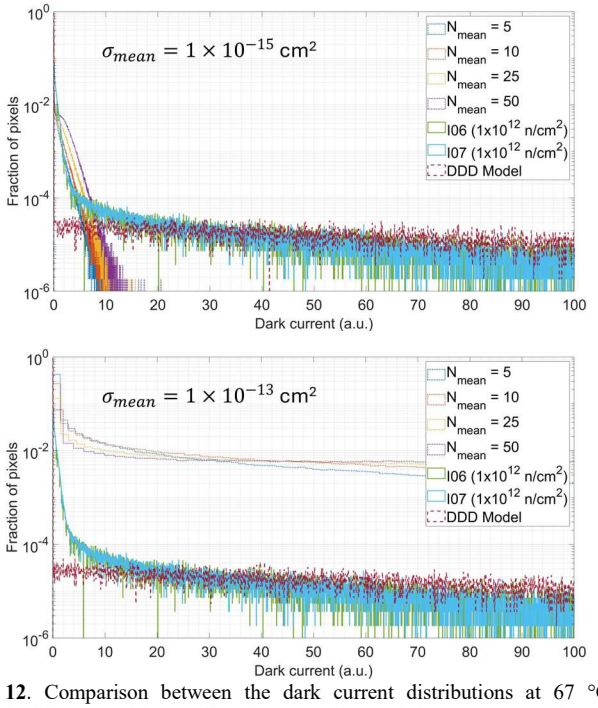

Fig. 12. Comparison between the dark current distributions at 67 °C obtained with our model as well as from experimental data (CIS I06 and I07). Also included is a DDD model for this fluence, as described in [24,25].

B. Modeling of DLTS spectra

In a similar vein, DLTS spectra can be modeled when considering the dependance of a trap's electron emissivities (e_n) on E_T, σ_n, and T, as described in [16]:

$$e_n = \sigma_n \cdot v_n \cdot N_c \cdot \exp\left(\frac{E_T - E_c}{kT}\right) \quad (9)$$

which can be rewritten in the following way when considering $v_n \propto T^{1/2}$ and $N_c \propto T^{3/2}$:

$$e_n = \sigma_n \cdot T^2 \cdot \frac{v_{n,300}(1.08)^{3/2}}{300^2} \cdot N_{c,0} \cdot \exp\left(\frac{E_T - E_c}{kT}\right) \quad (10)$$

with $v_{n,300} = 2.3 \times 10^7$ cm/s, and $N_{c,0} = 2.5 \times 10^{19}$ cm^{-3}.

Once the emissivity of a trap at a given temperature is calculated, its capacitance transient can be described, among others, by the quantity δC or ΔC, defined as the difference in capacitance of the depletion region between two times t_1 and t_2, after the end of the filling pulse, and before returning to a stationary value of C_∞. Assuming a trap density of N_T and an N-type doping concentration of N_D, ΔC is given by [27]:

$$\Delta C = C_\infty \left(\frac{N_T}{2N_D}\right) \cdot [exp(-t_2 e_n) - exp(-t_1 e_n)] \quad (11)$$

Theoretical DLTS spectra can thus be unequivocally simulated for point defects of interest, as is shown in Fig. 13. Five different point defects are considered to be simultaneously present in the depleted volume: C_iC_s, V_2, VP (also known as E-center) and C_iO_i, each with specific sharge states (two different ones in the case of V_2). Typical values were used for the constants, assuming an N-type Si Schottky diode: $C_\infty = 50$ pF and $N_D = 1 \times 10^{15}$ cm^{-3}. Similarly, arbitrary values in the order of several 10^{15} cm^{-3} were used for the assumed volumetric concentration of each trap. It can be observed that the peak position seems to have a strong correlation with the trap energy levels, with deeper traps having peaks at higher temperatures, and shallower ones at lower temperatures, with the peak amplitudes proportional to their respective concentrations. In this particular case, the three deepest traps have peaks very close to each other, and thus cannot be easily distinguished in the superimposed spectrum (shown with a dotted line) This represents a considerable difficulty when interpreting experimental DLTS results, although the capacitance transients associated with such close peaks are no longer necessarily described by an exponential function [9].

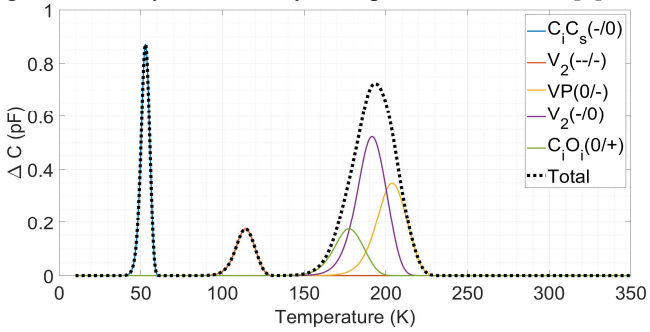

Fig. 13. Simulated DLTS spectra between 10 K and 350 K in N-type Si for five different traps: C_iC_s (-/0), V_2 (--/-), VP (0/-), V_2 (-/0) and C_iO_i (0/+). Trap parameters are taken from [4]: (E_T, σ_n) = (-0.11 eV, 4.0x10^{-14} cm^2), (-0.23 eV, 4.0x10^{-15} cm^2), (-0.47 eV, 3.6x10^{-14} cm^2), (-0.42 eV, 1.1x10^{-14} cm^2) and (-0.36 eV, 1.9x10^{-15} cm^2), respectively. Trap concentrations are arbitrarily chosen as 5x10^{13} cm^{-3}, 1x10^{13} cm^{-3}, 2x10^{13} cm^{-3}, 3x10^{13} cm^{-3} and 1x10^{13} cm^{-3}, respectively.

Under the same conditions, an attempt can be made to estimate the DLTS spectra produced by defect clusters present in the same depleted volume. Let us assume the presence of an arbitrary number of 100 distinct clusters, each of random size N, described by an exponential distribution rounded to the closest integer value as in (6), with $N_{mean} = 50$, one of the values used in Fig. 9. Each individual defect inside a cluster is assigned a couple of values E_T and σ_n, with uniform and exponential distributions, as before, with all of the defects assumed to be mutually independent. At a given temperature, the emissivity of each defect is calculated using (10), and the net emissivity of the cluster is calculated as follows:

$$\frac{1}{e_{n,cluster}} = \max_{1 \le i \le N}\left(\frac{1}{e_{n,i}}\right) \quad (12)$$

Fig. 14 shows the result of such a simulation, using a constant σ_{mean}, but varying the bounds of E_T, with the same values used in Fig. 11. N_T was estimated from the total number of defects in all simulated clusters, as well as a typical depleted volume of (1 mm^2)x(2 µm). In all three of the considered cases, the ΔC values obtained are dramatically lower than those of point defects in Fig. 13, with several orders of magnitude of difference. As shown, this difference can be slightly diminished either by reducing the range of E_T values or by removing the midgap altogether, such as in the bottom subplot. The difference remains very considerable nonetheless, and the contribution of clusters to DLTS spectra can then be considered

as noise in this particular case.

It should not be deduced from this that clusters generally have a negligible impact on the DLTS signatures measured experimentally for point defects. On the contrary, multiple previous studies have shown that the presence of clusters can affect features such as the relative amplitudes of DLTS peaks for certain traps, notably the divacancy in its shallow double-donor state [10,28]. In our model, however, simulated clusters are highly unlikely to contain a significant number of identical point defects, due to the uncorrelation between the randomly assigned values of E_T and σ_n.

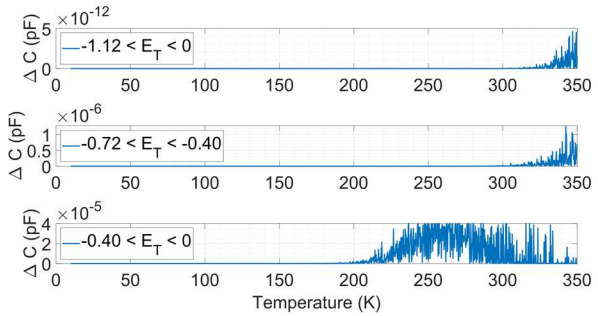

Fig. 14. Simulated DLTS spectra between 10 K and 350 K in N-type Si for 100 clusters of random size N, described by an exponential distribution with $N_{mean} = 50$. Each defect in a cluster has randomly assigned values of E_T (uniform distribution with bounds in the figure, in eV) and σ_n (exponential distribution with a mean value of 1×10^{-15} cm^2).

In general, DLTS spectra are more easily interpretable when there exists a high enough concentration in the depleted volume of identical point defects. The presence of clusters does not necessarily introduce a new DLTS signature per se, but it can in some cases modify the signatures of peaks inside or around the cluster region, and this influence is not so easily gauged.

C. General discussion – complementarity of the three spectroscopy techniques

In our study, the PL and DLTS techniques have presented the advantage of allowing easier access to the identifying spectral signatures of crystal defects in the silicon bulk, despite their lower sensitivity in comparison with DCS. This sensitivity is impacted, among others, by the parameters used during characterization. For the samples and photodiodes irradiated with neutrons at the highest fluences, our PL measurements evidenced the formation of optically active C_iO_i defects, whereas DLTS spectra revealed the presence of electrically active di-vacancies and potentially C_iC_s defects. The detection of these defects is likely dependent on the concentration of carbon and oxygen impurities in the irradiated volume, with the thickness of the top oxide layer also possibly playing a role. The fact that our DLTS results did not show any evidence of C_iO_i defects, which are supposed to be electrically active [29,30], might simply come from a potentially higher carbon or lower oxygen content in the PIN photodiodes, explaining a preferential formation of C_iC_s defects instead of C_iO_i defects. In the presence of clusters, the carbon and oxygen impurities necessary for the formation of these defects can also be originated from the cluster region, after being ejected from their initial substitutional sites following the annihilation of self-interstitials and vacancies inside the cluster [10].

In contrast, the DCS technique, despite being more strongly sensitive to the presence of defects in each of the sensor's microvolumes, can prove to be more challenging in identifying the spectral signatures of point defects, particularly in the presence of complex defect clusters, typically present after neutron irradiation involving significant displacement damage. Although these clusters are known to progressively anneal out with increasing temperature and post-irradiation time, some stable cluster configurations can still persist after these anneals, having a strong impact in dark current distributions due to the likelihood of the presence of energy levels close to the dominating midgap. Table III below summarizes the types of defects whose spectral signatures can be potentially observable with the DCS, DLTS and PL techniques, particularly applicable in the case of neutron irradiation.

Table III
Types of defects observable with DCS, DLTS and PL for neutron irradiation

Type of defect	Dark current / DCS	DLTS	PL
Single point defect	Yes	No	No
Shallow point defects (same type, large quantity)	Difficult (weak dark current)	Yes	Yes
Deep point defects (same type, large quantity)	Yes	Yes	No (depends on the detector)
Irradiation-induced defect clusters	Yes (midgap centers dominate)	Hardly	No
Point defects if presence of clusters	Hardly	Yes	Yes (if shallow)

In the case of PL results, it should be mentioned that the energy of emitted photons does not necessarily correspond exactly to the associated trap energy levels in the bandgap for an indirect gap semiconductor such as silicon. There exists in fact a difference between the absorbed and emitted photon energies, the so-called Stokes shift [31]. This shift represents the phononic transitions necessary due to the different equilibrium atomic configurations in the excited and ground states of the defect. The energy of photons emitted during PL measurements is thus not so easily comparable with energy descriptors obtained from electrical measurements such as DLTS and DCS, in particular their activation energy which is more closely related to the trap energy levels. Despite this, PL can still prove to be very useful in the context of the identification of irradiation-induced defects in silicon, especially when used in conjunction with other spectroscopy techniques, or with the aid of theoretical calculations.

In general, in the context of the identification of the kinds of defects generated by neutron irradiation in silicon, the three techniques are complementary and provide useful information, despite their specific limitations.

V. Conclusion

Our study showed that neutron irradiations with fluences of

at least 1×10^{10} cm^{-2} were sufficient to generate an exponential tail of white pixels in the dark current distributions of CIS under test, with the DCS-extracted activation energy having values close to the middle of the bandgap for high dark current values. PL and DLTS measurements on samples irradiated under the same conditions suggested respectively the possible presence of optically active CiOi defects and electrically active C_iC_s defects and di-vacancies (in its double charged state); the observation of the former two is likely dependent on the carbon and oxygen concentrations in the bulk silicon. Under our experimental conditions, these PL and DLTS measurements required higher neutron fluences of respectively 1×10^{11} cm^{-2} and 5×10^{10} cm^{-2} for the defect signatures to be detectable, indicating a lower sensitivity that in the case of DCS. The point defects detected using the PL and DLTS techniques are relatively shallow, and thus not the most likely candidates to explain the exponential tails observed in the dark current distributions, probably originated instead by complex clusters of interstitials and vacancies, as already proposed in the literature [2,3].

A simplified model is proposed to fit the general characteristics of known experimental DCS and DLTS spectra for both populations of identical point defects as well as defect clusters. In the case of point defects, their exclusive presence in a CIS can be described with a Poisson distribution, and they can lead to quantized peaks in DCS spectra if the number of defects per pixel is sufficiently low. These point defects are also responsible for well-defined gaussian peaks in DLTS spectra when in high enough concentrations, and their peak position is at higher temperatures when the traps have deeper levels. In contrast, our model considers clusters as agglomerations of mutually independent point defects, with randomly assigned energy levels and capture cross sections, following respectively a uniform and an exponential distribution. Under these assumptions, and assuming that the size of the clusters is also ruled by an exponential distribution, we simulate exponential tails of hot pixels in DCS spectra, with qualitatively similar characteristics to experimental data. The same model shows that clusters only have a small-amplitude noisy contribution to DLTS spectra, although they are known experimentally to be able to affect the signatures of some point defects present in the cluster region.

In this study, the DCS, DLTS and PL characterization techniques have proven to be valuable and complementary not in spite of but because of their respective abilities to detect the signatures of different kinds of defects generated in the bulk silicon after neutron irradiation. Despite not providing energy levels in the bandgap in a straightforward manner, PL spectra provides useful indications of optically active defects that may prove deleterious for the performance of silicon-based CMOS image sensors.

ACKNOWLEDGEMENT

This work was partially supported by the LAAS-CNRS micro and nanotechnologies platform, a member of the French Renatech network. The authors would also like to thank the Centre national d'études spatiales as well as the Cyclotron Resources Centre at UCLouvain for their support in conducting the neutron irradiation campaign necessary for this study.

REFERENCES

[1] Z. Wang *et al.*, "Radiation effects in backside-illuminated CMOS image sensors irradiated by high energy neutrons at CSNS-WNS," *Nucl. Inst Methods Phys. Res. A*, vol. 1026, no. 166154, pp. 1–6, 2022, doi: https://doi.org/10.1016/j.nima.2021.166154.

[2] X. Zhang *et al.*, "Displacement damage effects induced by fast neutron in backside-illuminated CMOS image sensors," *J. Nucl. Sci. Technol.*, vol. 57, no. 9, pp. 1015–1021, 2020, doi: https://doi.org/10.1080/00223131.2020.1751323.

[3] A. L. Roch *et al.*, "Phosphorus Versus Arsenic: Role of the Photodiode Doping Element in CMOS Image Sensor Radiation-Induced Dark Current and Random Telegraph Signal," *IEEE Trans. Nucl. Sci.*, vol. 67, no. 7, 2020.

[4] P. Kaminski, R. Kozlowski, and E. Nossarzewska-Orlowska, "Formation of electrically active defects in neutron irradiated silicon," *Nucl. Instrum. Methods Phys. Res. B*, vol. 186, pp. 152–156, 2002.

[5] M. Moll, H. Feick, E. Fretwurst, G. Lindstrom, and C. Schutze, "Comparison of defects produced by fast neutrons and 60Co-gammas in high-resistivity silicon detectors using deep-level transient spectroscopy," *Nucl. Instrum. Methods Phys. Res. A*, vol. 388, pp. 335–339, 1997.

[6] B. Liu *et al.*, "Displacement Damage Effects in Backside Illuminated CMOS Image Sensors," *IEEE Trans. ELECTRON DEVICES*, vol. 69, no. 6, 2022.

[7] V. Malherbe *et al.*, "Radiation Characterization of a Backside-Illuminated P-Type Photo-MOS Pixel With Gamma Rays and Fusion-Induced Neutrons," *IEEE Trans. Nucl. Sci.*, vol. 69, no. 3, pp. 534–541, 2022, doi: 10.1109/TNS.2022.3148925.

[8] J.-M. Belloir *et al.*, "Dark Current Spectroscopy in neutron, proton and ion irradiated CMOS Image Sensors: from Point Defects to Clusters," *IEEE Trans. Nucl. Sci.*, vol. 64, pp. 27–37, 2016.

[9] Olivié, François, "MOS ULTIMES - Contribution à la technologie des transistors MOS ultimes : oxydes minces, préamorphisation, défauts," Université de Toulouse, 1999.

[10] R. M. Fleming, C. H. Seager, D. V. Lang, Cooper P J, Bielejec, E, and Campbell, J M, "Effects of clustering on the properties of defects in neutron irradiated silicon," *J Appl Phys*, vol. 102, no. 043711, pp. 1–13, 2007.

[11] A. Junkes, D. Eckstein, I. Pintilie, L. F. Makarenko, and E. Fretwurst, "Annealing study of a bistable cluster defect," *Nucl. Instrum. Methods Phys. Res. A*, vol. 612, pp. 525–529, 2010.

[12] H. Kiuchi *et al.*, "Determination of low carbon concentration in Czochralski-grown Si crystals for solar cells by luminescence activation using electron irradiation," *Jpn J Appl Phys*, vol. 56, 2017, doi: https://doi.org/10.7567/JJAP.56.070305.

[13] K. Thonke, Hangleiter, A, J. Wagner, and R. Sauer, "0.79 eV (C line) defect in irradiated oxygen-rich silicon: excited state structure, internal strain and luminescence decay time," *J Phys C Solid State Phys*, vol. 18, 1985.

[14] V. Bondarenko, R. Krause-Rehberg, H. Feick, and C. Davia, "Defects in FZ-silicon after neutron irradiation—A positron annihilation and photoluminescence study," *J. Mater. Sci.*, vol. 39, pp. 919–923, 2004.

[15] M. Tajima, Asahara, Shota, Satake, Yuta, and Ogura, Atsushi, "Free-to-bound emission from interstitial carbon and oxygen defects (CiOi) in electron-irradiated Si," *Appl Phys Express*, vol. 14, no. 011006, pp. 1–4, 2021, doi: https://doi.org/10.35848/1882-0786/abd4c6.

[16] F. Domengie, "Etude des défauts électriquement actifs dans les matériaux des capteurs d'image CMOS," PhD Thesis, Université de Grenoble, 2011.

[17] F. Domengie, J. L. Regolini, and D. Bauza, "Study of Metal Contamination in CMOS Image Sensors by Dark-Current and Deep-Level Transient Spectroscopies," *J. Electron. Mater.*, vol. 39, no. 6, pp. 625–629, 2010.

[18] W. C. McColgin, J. P. Lavine, and Stancampiano, C V, "Probing metal defects in CCD image sensors," in *Materials Research Society Symposium Proceedings*, 1995, pp. 713–724.

[19] ASTM, “Standard Practice for Characterizing Neutron Fluence Spectra in Terms of an Equivalent Monoenergetic Neutron Fluence for Radiation-Hardness Testing of Electronics, ASTM International Std. E722-19.” 2019. [Online]. Available: https://www.astm.org/e0722-19.html

[20] Vasilescu, A and Lindstroem, G, “Displacement damage in silicon, on-line compilation.” [Online]. Available: https://rd50.web.cern.ch/NIEL/

[21] M. Raine, A. Jay, N. Richard, V. Goiffon, and S. Girard, “Simulation of Single Particle Displacement Damage in Silicon – Part I: Global Approach and Primary Interaction Simulation,” *IEEE Trans. Nucl. Sci.*, vol. 64, no. 1, 2017.

[22] A. Jay *et al.*, “Simulation of Single Particle Displacement Damage in Silicon – Part II: Generation and Long-Time Relaxation of Damage Structure,” *IEEE Trans. Nucl. Sci.*, vol. 64, pp. 141–148, 2017.

[23] J. R. Srour and D. H. Lo, “Universal damage factor for radiation-induced dark current in silicon devices,” *IEEE Trans. Nucl. Sci.*, vol. 47, no. 6, 2000.

[24] A. L. Roch *et al.*, “Radiation-Induced Leakage Current and Electric Field Enhancement in CMOS Image Sensor Sense Node Floating Diffusions,” *IEEE Trans. Nucl. Sci.*, vol. 66, no. 3, 2019, doi: 10.1109/TNS.2019.2892645.

[25] J.-M. Belloir *et al.*, “Pixel pitch and particle energy influence on the dark current distribution of neutron irradiated CMOS image sensors,” *Opt. EXPRESS*, vol. 24, no. 4, pp. 4299–4315, 2016, doi: 10.1364/OE.24.004299.

[26] A. Jay *et al.*, “Clusters of Defects as a Possible Origin of Random Telegraph Signal in Imager Devices: a DFT based Study,” in *2021 INTERNATIONAL CONFERENCE ON SIMULATION OF SEMICONDUCTOR PROCESSES AND DEVICES (SISPAD 2021)*, 2021, pp. 128–132. doi: 10.1109/SISPAD54002.2021.9592553.

[27] D. V. Lang, “Deep-level transient spectroscopy: A new method to characterize traps in semiconductors,” *J Appl Phys*, vol. 45, no. 7, pp. 3023–3032, 1974.

[28] I. Pintilie, G. Lindstroem, A. Junkes, and E. Fretwurst, “Radiation-induced point- and cluster-related defects with strong impact on damage properties of silicon detectors,” *Nucl. Instrum. Methods Phys. Res. A*, vol. 611, pp. 52–68, 2009, doi: 10.1016/j.nima.2009.09.065.

[29] A. Himmerlich *et al.*, “Defect characterization studies on irradiated boron-doped silicon pad diodes and Low Gain Avalanche Detectors,” *Nucl. Inst Methods Phys. Res. A*, vol. 1048, 2023, doi: https://doi.org/10.1016/j.nima.2022.167977.

[30] E. Gaubas, D. Bajarūnas, T. Čeponis, D. Meškauskaitė, and J. Pavlov, “OPTICALLY INDUCED CURRENT DEEP LEVEL SPECTROSCOPY OF RADIATION DEFECTS IN NEUTRON IRRADIATED Si PAD DETECTORS,” *Lith J Phys*, vol. 53, no. 4, pp. 215–218, 2013.

[31] A. Alkauskas, M. D. McCluskey, and Van de Walle, Chris G, “Tutorial: Defects in semiconductors—Combining experiment and theory,” *J Appl Phys*, vol. 119, no. 181101, pp. 1–11, 2016, doi: http://dx.doi.org/10.1063/1.4948245.